Geophys. J. Int. (2002) **151,** 279–295

The lowermost mantle beneath northern Asia—I. Multi-azimuth studies of a D″ heterogeneity

Ch. Thomas,[1,*] J.-M. Kendall[2] and M. Weber[3]

[1] *Department of Earth Sciences, University of Liverpool, Liverpool,* L69 3GP, *UK*
[2] *Department of Earth Sciences, University of Leeds, Leeds,* L52 9JT, *UK*
[3] *GeoForschungsZentrum Potsdam, Telegraphenberg, House,* 14473 *Potsdam, Germany*

Accepted 2002 May 8. Received 2002 April 26; in original form 2000 December 5

SUMMARY

In most areas of the globe it is only possible to sample the lowermost mantle or D″ region with a limited range of azimuths. This is due to limitations in source–receiver geometries. An exception is the region beneath northern Siberia where we are able to sample D″ along orthogonal great-circle paths using northern-Pacific earthquakes recorded in Europe and Hindu-Kush earthquakes recorded in Canada. Receiver vespagrams (slant stacks of one source recorded at many receivers) for a Kurile event recorded at the German Regional Seismic Network (GRSN) and the Gräfenberg-array and source vespagrams (many sources, one receiver) of Hindu-Kush events recorded at stations of the Canadian National Seismograph Network (CNSN) show reflections from a discontinuity at the top of D″. Vespagrams for real data are compared to vespagrams for synthetic data in order to guide their interpretation. Additional support for our interpretation comes from frequency-wavenumber ($f-k$) analysis which provides a measure of the slowness and azimuth of a given phase. The traveltimes of the D″ reflected phases are then used to provide estimates of D″ thickness. In regions where the roughly orthogonal paths overlap we estimate the thickness to be 310 (±15) km, which is in agreement with existing models for this region. We also estimate a thickness of 210 (±15) km in a previously unsampled region east of this area. Using the slowness, backazimuth and traveltime values for a third source–receiver combination, we find a reflection point at a depth of 2800 km (thickness of D″ of 91 km) in a region several degrees to the west. These results and those of previous studies suggest considerable topographic relief (100 km) over distances of less than 5° (approximately 300 km at the CMB). Comparing the results from this study with results from other seismic studies of D″ structure in this area, we find this to be a complicated region which exhibits heterogeneity on many scales. This region may be the lower-mantle graveyard of the subducted Izanagi plate and one interpretation of this complexity is that it is due to subduction related deformation at the base of the mantle.

Key words: array methods, lower mantle, *P* waves, seismology.

1 INTRODUCTION

Seismic studies of the structure of the D″ region (i.e. lowermost few 100 kms of the mantle) provide important insights into core and mantle processes such as slab penetration into the lower mantle, plume formation at the core–mantle boundary (CMB) and convection in the core and mantle (for reviews see e.g. Loper & Lay 1995; Weber *et al.* 1996). The region beneath northern Siberia is an especially well studied area. Past studies have investigated a discontinuity at the top of the D″ layer using northwest-Pacific earthquakes recorded by European seismic networks (e.g. Lay & Helmberger 1983; Weber & Davis 1990; Gaherty & Lay 1992; Houard & Nataf 1993). Primary evidence for this discontinuity comes from observations of *PcP* and ScS precursors which are interpreted as reflections at near-critical incidence angles to the discontinuity. There has, though, been some controversy over this interpretation and near-source effects have been suggested as alternate interpretations (Haddon & Buchbinder 1986). In general, limitations in source–receiver geometries make it highly unusual to be able to study this discontinuity with more than a limited range of source–receiver azimuths. Here we analyse *P*-waves from earthquakes in the Hindu Kush region recorded in Canada which fortuitously have source–receiver azimuths roughly orthogonal to the NW-Pacific-to-Europe paths (Fig. 1). Confirmation of the discontinuity beneath Siberia from another azimuth provides an additional way of ruling out alternate explanations for the anomalous seismic signals (e.g. source region structure).

*Previously at: Department of Earth Sciences University of Leeds, UK.

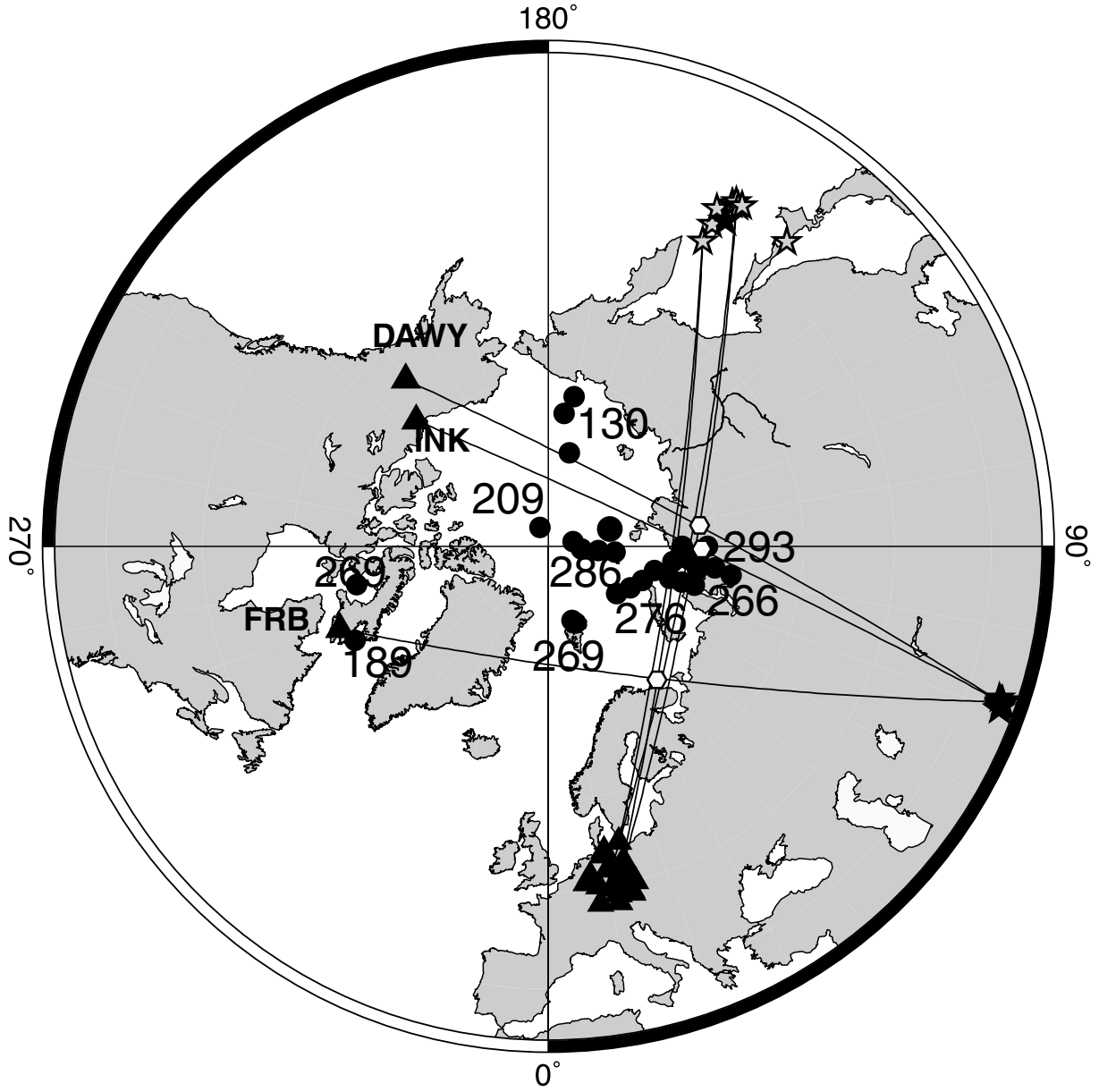

Figure 1. Source–receiver geometries used to study D″ beneath northern Siberia. Earthquakes in Japan, the Kuriles and the Hindu-Kush region are indicated by stars, with the black stars showing the events presented in this study. Black triangles show the stations of the Canadian National Seismograph Network (CNSN), the German Regional Seismograph Network (GRSN) and the GRF-array used in this study. Estimates of D″ thickness from previous *P*-wave studies are indicated near the solid circles (see text for references to previous work). The grey hexagons indicate the regions imaged by the paths between the Hindu Kush region and Canada.

A conventional receiver vespagram (slant stack of one source recorded at many receivers) (Davies *et al.* 1971) is produced for the NW-Pacific-to-Europe path and source vespagrams (many sources, one receiver) are produced for the Hindu-Kush-to-Canada path. We also use a frequency-wavenumber ($f - k$) technique (e.g. Capon 1973) which provides a means of simultaneously estimating the slowness and arrival azimuth of a given phase. This approach has seldom been used to study D″ reflections (e.g. Weber 1993). Estimates of the thickness of D″ for the new path, Hindu-Kush-to-Canada, show good agreement with the estimates for the NW-Pacific-to-Europe paths. We also sample the discontinuity in a previously untested region (see hexagon in Fig. 1 between FRB and Hindu Kush). The observations are compared to results from synthetic data for models with and without D″.

Other means of studying the structure of the core–mantle transition zone are, for example, investigations of scattered waves which arrive as precursors to the core phase *PKPdf* (e.g. Cleary & Haddon 1972; Vidale & Hedlin 1998; Wen & Helmberger 1998; Thomas *et al.* 1999) or ultra-low velocity zones at the base of the mantle (e.g. Garnero *et al.* 1998). In the final section we contrast and compare our results with those from such complementary investigations.

2 DATA

We analyse earthquakes from the Hindu Kush region recorded by the Canadian National Seismograph Network (CNSN) and reanalyse an earthquake from the Kurile Islands recorded by the German

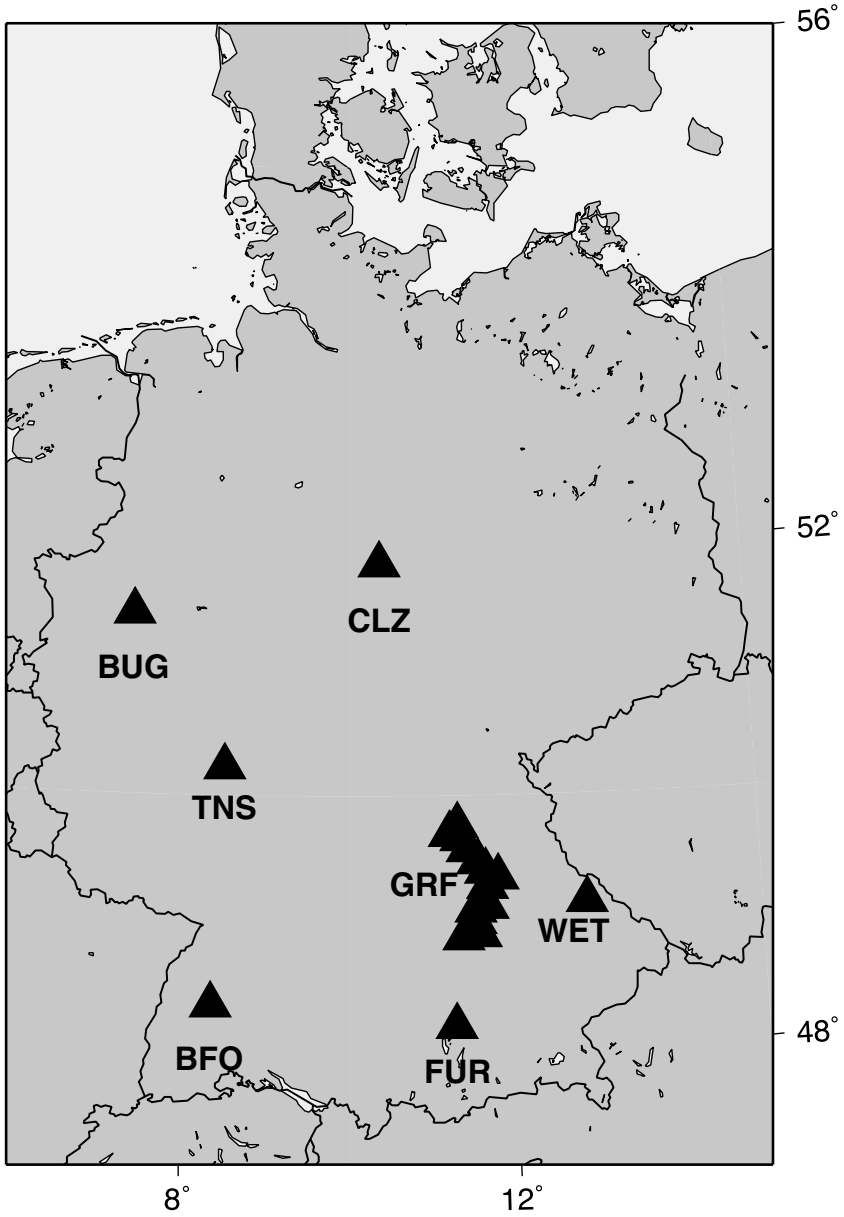

Figure 2. The station distribution of the German Regional Seismic Network (GRSN) and the Gräfenberg array (GRF) used in this study.

Regional Seismic Network (GRSN) and the stations of the Gräfenberg-Array (GRF) located in southern Germany (from Thomas & Weber 1997). The sources and receivers are shown in Fig. 1. The stations of the GRSN and GRF used in this study are shown in Fig. 2. These source–receiver combinations sample an area beneath northern Siberia with propagation paths which are almost perpendicular to each other. Estimates of D″ thickness from previous studies (Scherbaum *et al.* 1997) are also shown in Fig. 1.

The stations of the CNSN, the GRSN and the GRF-array are equipped with three-component broad-band seismometers which record ground velocity. Data recorded at these stations are analysed using vespagrams and stacking in the frequency—wavenumber ($f - k$) domain. Coherency in waveforms is crucial in these techniques and this is ensured by visual inspection of each waveform. We find the station spacing and aperture of the GRF and a subset of GRSN stations small enough for coherence in *P*-waveforms recorded from a deep-focus event in the Kurile subduction region (Table 1, #20). Thomas & Weber (1997) and Thomas *et al.* (1999) also found coherency in waveforms recorded across these arrays. The slowness resolution for the used sub-set of stations from the GRSN is much better than it is for the much smaller GRF array (see example below).

The CNSN stations, on the other hand, are spaced too far apart for such analysis using receiver arrays. Instead we use a source array where many events are slant stacked at one station producing a source vespagram (Krüger *et al.* 1995). As with the German receiver array, we also stack in the $f - k$ domain using this source array. The epicentres of events in the Hindu Kush region are shown in Fig. 3. Such source stacking works best if the events are almost at the same depths; we therefore use events with source depths near 200 km. Shallow events from this region could not be used as a source array because their epicentres are too far apart for coherency in waveforms. The parameters for the Hindu-Kush events used are listed in Table 1 (#1–19).

Table 1. Events used in this study. Earthquake parameters are from the Preliminary Determination of Earthquakes (PDE) list.

#	Date	Time	Lat	Lon	h	Magnitude	Average distance		
	yy/mm/dd	hh:mm:ss.t			(km)		DAWY	INK	FRB
1	93/08/09	11:38:30.5	36.44	70.71	204	6.4 Mw	77.04	74.02	75.24
2	93/08/09	12:42:48.2	36.38	70.87	214	7.0 Mw	77.07	74.06	75.34
3	93/09/04	11:38:38.9	36.43	70.81	194	6.0 Mw	77.03	74.02	75.27
4	94/06/30	09:23:21.4	36.33	71.13	226	6.5 mb	77.07	74.08	75.45
5	94/10/25	00:54:34.3	36.36	70.96	238	6.2 mb	77.07	74.07	75.38
6	95/05/16	03:35:02.6	36.46	70.89	186	5.9 Mw	76.98	73.98	75.27
7	95/08/17	23:14:19.0	36.44	71.13	233	5.6 Mw	76.96	73.97	75.34
8	95/10/18	09:30:38.5	36.43	70.39	222	6.3 Mw	77.11	74.07	75.17
9	95/12/25	03:19:44.9	36.45	70.21	228	5.6 Mw	77.12	74.07	75.11
10	97/05/13	14:13:45.7	36.41	70.94	196	6.5 Mw	77.03	74.02	75.33
11	97/05/15	18:30:24.2	36.40	70.86	184	5.0 mb	77.05	74.04	75.31
12	97/12/17	05:51:29.2	36.39	70.77	207	6.3 Mw	77.08	74.06	75.30
13	98/02/14	00:08:07.8	36.36	71.11	218	5.5 Mw	77.04	74.05	75.41
14	98/02/20	12:18:06.2	36.48	71.09	235	6.4 Mw	76.93	73.93	75.30
15	98/03/21	18:22:28.5	36.43	70.13	227	6.0 Mw	77.15	74.10	75.11
16	98/12/11	20:16:24.0	36.51	71.02	222	5.7 Mw	76.91	73.91	75.25
17	99/02/09	17:33:16.7	36.38	70.75	192	5.3 Mw	77.09	74.07	75.31
18	99/06/21	17:37:27.2	36.39	70.71	230	5.5 Mw	77.09	74.07	75.29
19	99/06/29	23:18:05.6	36.62	71.35	189	5.9 mb	76.75	73.76	75.23
20	91/12/17	06:38:17.3	47.39	151.50	157	5.8 mb		–	

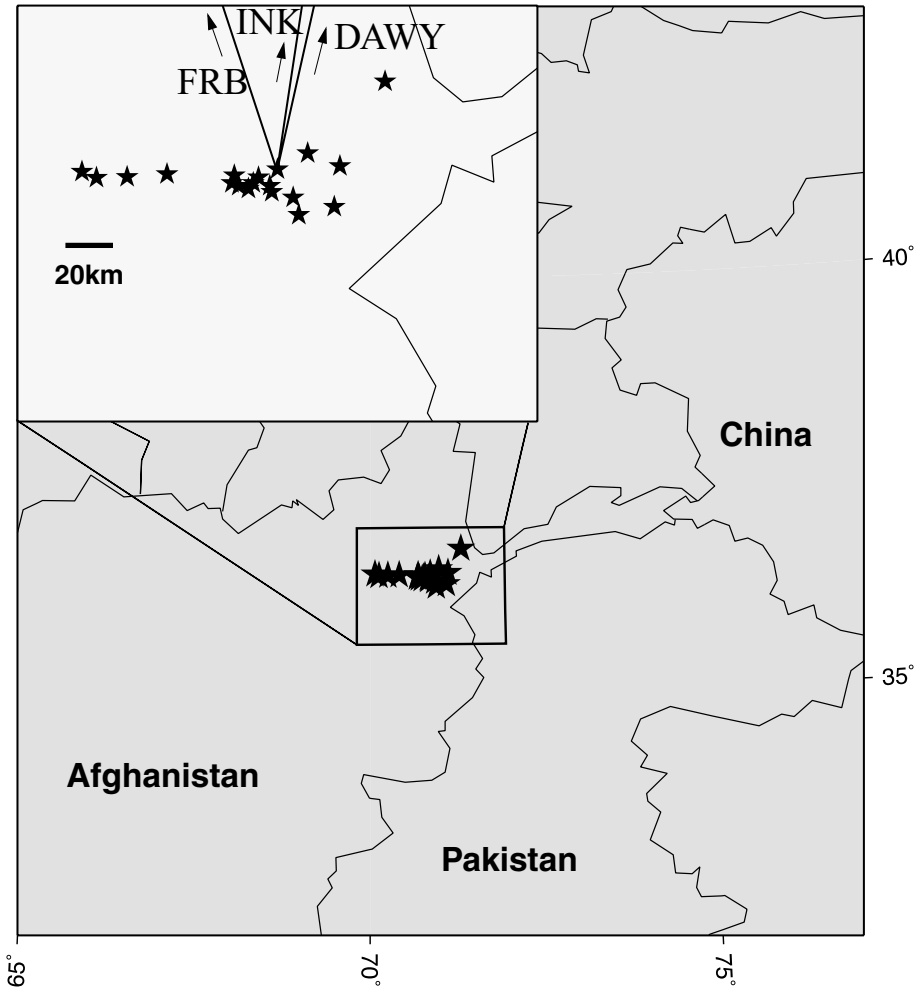

Figure 3. Epicentres of events in the Hindu Kush region. The black stars show epicentres of events used in this study. The insert in the top left corner shows the location of the deep events given in Table 1. The region covered by these events is approximately 50 × 120 km. The great circle azimuths to the CNSN stations FRB, INK and DAWY azimuths are shown in the insert.

Table 2. Measured and theoretical slowness (u) and back azimuth (baz) values for *P*, *PdP* and *PcP* and traveltimes relative to *P*. The model PREM has been used to calculate theoretical values.

		P		*PdP*			*PcP*	
		u	Baz	u	Baz	Rel.tt	u	Rel.tt
GRSN	vespa	5.6	–	4.9 (±0.2)	–	4.5	–	–
	$f-k$	5.6 (±0.5)	26.8 (±11)	4.9 (±0.5)	27.8 (±11)		–	
	theo.	5.6	26.8	4.9	26.8	5.5	4.3	12
DAWY	vespa	5.6	–	5.3 (±0.4)	–	7	4.6 (±0.4)	11
	$f-k$	5.6 (±0.8)	12.7 (±5)	5.2 (±1.2)	12.2 (±8)		–	
	theo.	5.6	13	4.75 (±0.3)	13	7	4.3 (±0.3)	12
INK	vespa	5.8	–	5.5 (±1.2)	–	6.75	4.3 (±1.5)	13.5
	$f-k$	5.8 (±0.8)	9 (±5)	5.2 (±2.5)	8 (±13)		–	
	theo.	5.8	9	5.0 (±0.3)	9	6.75	4.3 (±0.3)	14
FRB	vespa	5.7	–	5.2 (±0.4)	–	7.35	–	–
	$f-k$	5.7 (±1.0)	342 (±5)	3.9 (±2.5)	327 (±35)		–	
	theo.	5.7	342	4.9 (±0.3)	342	7.35	4.3 (±0.3)	12

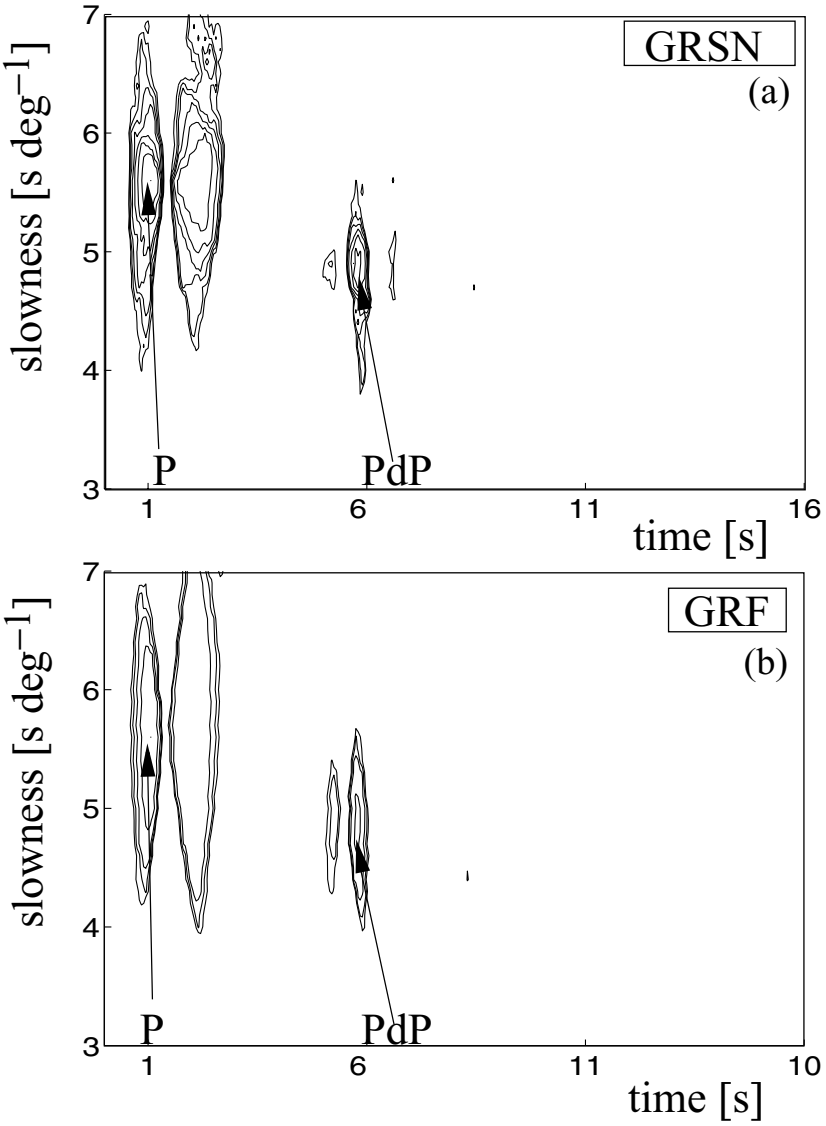

Figure 4. (Top) A Nth root ($N = 4$) receiver vespagram for the vertical component of GRSN and GRF stations for a Kurile event (#20 in Table 1) which is on average 76° from the stations. The traces are broadband recordings. Contour lines give amplitude in −3dB steps. The error was estimated using the −3dB line for each phase. The *PdP* phase arrives about 4.5 s after *P* with a slowness 0.7(±0.2) s/° less than *P*(5.6 s/°). (Bottom) An Nth root ($N = 4$) vespagram of the 13 GRF stations only of the same event. The slowness resolution of the phases is less compared to a vespagram of the whole GRSN (±0.6 s/° compared to ±0.2 s/°).

The insert in Fig. 3 shows that the epicentres of the deep Hindu-Kush events, our source array, cover a region 50 × 120 km which is comparable to the aperture of the GRF array. But the long axis of this source array trends roughly east-west, an orientation which is nearly perpendicular to the great-circle paths to the CNSN stations. This reduces the slowness resolution of this array. In contrast, the GRSN and GRF-array are more symmetrical in shape and consequently give better slowness resolution for the Kurile event recorded by the receiver vespagram. Another disadvantage of a source array is that phases which are sensitive to near receiver structure also appear as coherent energy and thereby potentially mask the D″ signals. Such signals are attenuated in a receiver vespagram due to differences in the near-receiver structure between stations. For example, variations in Moho depth between stations of the GRSN, would mask Moho reverberations in receiver stacks. Source stacks at a single receiver would accentuate them.

3 VESPAGRAM ANALYSIS

An Nth root ($N = 4$) *P*-wave receiver slowness vespagram (hereafter called vespagram) of broad-band data for the Kurile event (#20) recorded at the GRSN and GRF-array is shown in Fig. 4. The average epicentral distance is 76°. The Nth root technique is a robust nonlinear signal detection technique (Muirhead & Datt 1976) which is applied to improve the signal-to-noise ratio and allows better determination of the slowness of the different phases in the vespagrams. Should a discontinuity exist, a D″ reflection, PdP, will lie between the *P* and *PcP* phases with respect to both time and slowness.

In the GRSN vespagram a PdP phase can be seen roughly 4.5 s after *P* with a slowness of 4.9 s/° (±0.2 s/°), 0.7 s/° smaller than that for *P* (5.6 ± 0.2 s/°). Following the convention adopted in Weber and Davis (1991), errors were measured from the 3dB line (−30 per cent

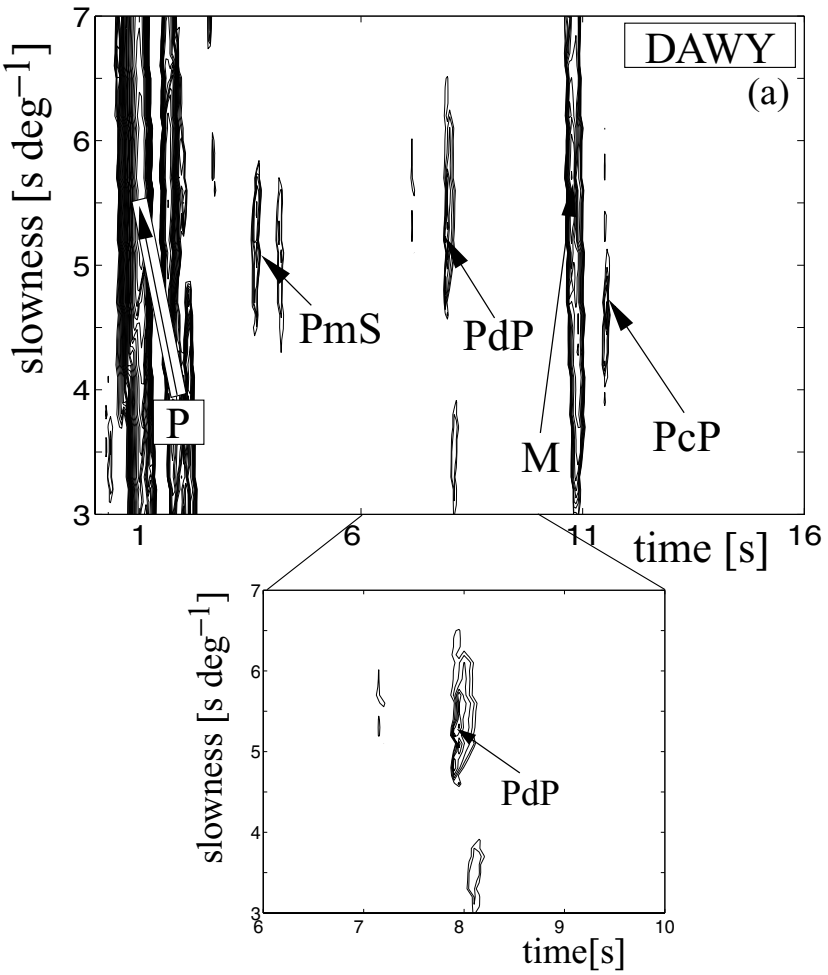

Figure 5. (a) An Nth root ($N = 4$) source vespagram for the vertical traces (broad-band velocity) of 14 Hindu-Kush events recorded at the station CNSN station DAWY with an average epicentral distance of 77°. The *P* wavelets are similar for most of the events. Events with a different *P* wavelet were not used for producing vespagrams. Events 1, 3–10, 13–15 and 18–19 were used to produce this vespagram. The selection of events depends on coherency of *P*-waves and availability of data. Indicated slowness values are from a model with a reflector 300 km above the CMB. *PdP* appears 7 s after *P* with a reduced slowness. The other phases are a *P* to *S* conversion at the Moho (PmS) and the Moho multiples (M). *PcP* arrives at the same time as the Moho multiple. Contours as in Fig. 4. (b) Vespagram of synthetic data for the model shown in Fig. 6(a) without a D″ discontinuity. The phases after *P* are the *P* to *S* conversion at the Moho and the Moho multiple as well as *PcP*. In the time window 7 s after *P* no additional phase arrives in contrast to the real data. (c) As (b) but for the model with a D″ discontinuity. Here an additional phase arrives 7 s after *P* which is due to the reflection from the top of D″. (d) As (c) but for a smaller array (40 km, 7 'sources').

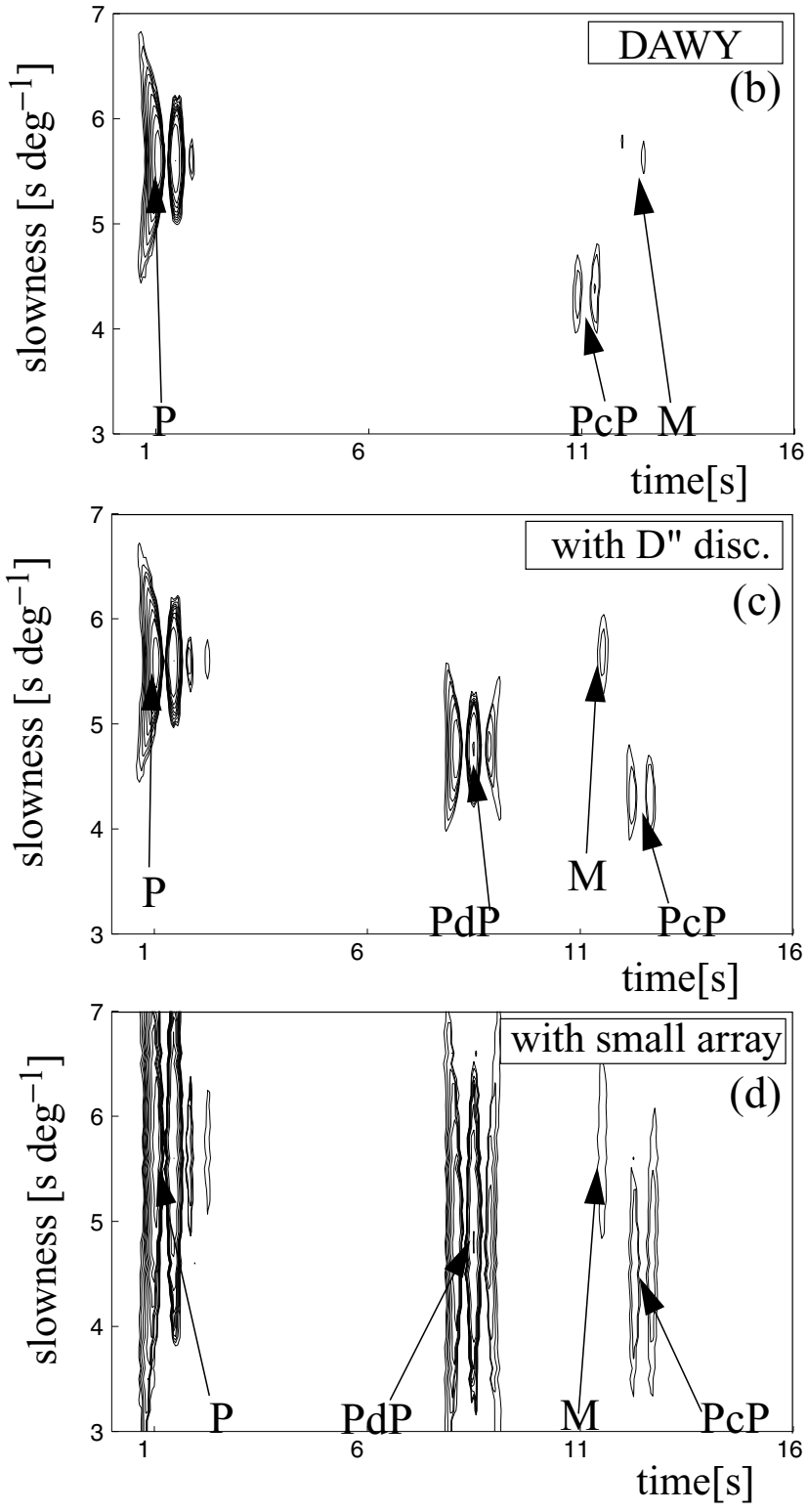

Figure 5. (*Continued*).

of the maximum amplitude) which is the first contour line in Fig. 4.

The amplitude of PdP is almost as large as the amplitude of *P* (4dB smaller than the *P* amplitude). In fact, this phase is visible on the individual seismograms before stacking. The core–mantle boundary (CMB) reflection, *PcP*, is not visible due to a small reflection coefficient but its theoretical arrival time would be roughly 12 s after *P* with a slowness 1.3 s/° smaller than *P*. Table 2 shows the measured and theoretical values.

Comparing results for the GRSN array and the GRF array reveals that the slowness resolution is reduced in the GRF vespagram (±0.6 s/°). This is due to the smaller aperture of the GRF

array (50 × 100 km) compared to that of the used part of the GRSN (350 km × 350 km).

In this study, the thickness of the D″ layer is estimated from the PdP arrival times in the vespagrams. This is done by modifying the thickness of the D″ region in the model PWDK (Weber & Davis 1990) which was developed for the region. For the Kurile event (Fig. 4a) the thickness of D″ lies within the error (±10 km) of the model PWDK (reflector at 2605 km depth or a thickness of 293 km, (Weber & Davis 1990) as estimated by (Thomas & Weber 1997).

Three stations in the CNSN were within the appropriate distance range to search for D″ reflectors (between ∼65° and ∼83°). We show source vespagrams for the stations DAWY (Dawson City, Yukon), INK (Inuvik, NWT) and FRB (Frobisher Bay); the average epicentral distances are 77°, 74° and 75° respectively. These vespagrams are expected to be more complicated than receiver vespagrams as near-receiver phase conversions and reverberations will also stack coherently at each station. Therefore, in order to guide the data interpretation we compare the vespagrams with those generated from synthetic data for models with and without a discontinuity at the top of D″. The synthetic data were produced using the reflectivity method (Müller 1985) with the reference model PREM (Dziewonski & Anderson 1981) and the focal mechanism of one of the Hindu-Kush events (event 6 in Table 1). It should be noted that there is little variation in the source mechanisms for the deep events we have chosen. The model was perturbed to include the near-surface structure at each station and the best fitting D″ discontinuity thickness. The advantage of the reflectivity method is that it is a full wavefield modelling method and therefore includes all phases that are generated by a discontinuity at the top of D″.

The source vespagrams for real and synthetic data for the station DAWY are shown in Fig. 5. The crustal structure for this station (Lowe & Cassidy 1995) (Fig. 6a) is used to predict the near-surface phases in the *P* coda: a *P* to *S* conversion at the Moho discontinuity ∼3 s after *P*; a Moho multiple with a similar slowness as *P* (5.6 s/°) ∼10 s after *P*. Finally *PcP* should have a slowness of 4.3 s/° and lag 12 s behind *P* and therefore start to interfere with the larger Moho multiple. The measured arrival time in the data is 11 s after *P* and the slowness is 4.6 (±0.4 s/°).

The real data (Fig. 5a) show an additional phase 7 s after *P* which has a slowness of about 5.3 s/° (±0.4 s/°) and is interpreted as a D″ reflection. The estimated D″ thickness for the arrival time of *PdP* with respect to *P* is 210 ± 15 km. All measurements have been made relative to the *P* wave slowness and backazimuth where the value of 5.6 s/° for the slowness and 13° for the backazimuth have been assigned to the *P* wave. A vespagram for a model without a D″ discontinuity is shown in Fig. 5(b) and one with a D″ discontinuity at this height above the CMB and a 3 per cent jump in velocity is shown in Fig. 5(c). The synthetic vespagrams are produced using stations in a distance range of 76.5–77.5° with a 0.1° spacing distributed along a line. This is a larger distance range than the distance range of the Hindu-Kush events recorded at DAWY (76.75°–77.15°) in the direction of the great circle path. As a result the slowness resolution of the vespagram using synthetic data is better than that of the real data (error: ±0.3 s/°). The slowness of the synthetic *PdP* phase is 4.75 (±0.3) s/° and it arrives 7 s after *P*. This arrival time agrees well with the observations in the vespagram for the real data. To demonstrate the effect of the size of the source array in the direction of the great circle path we show a vespagram for an array with an aperture of 40 km for synthetic data which corresponds better with the size of the real array (Fig. 5d). The slowness

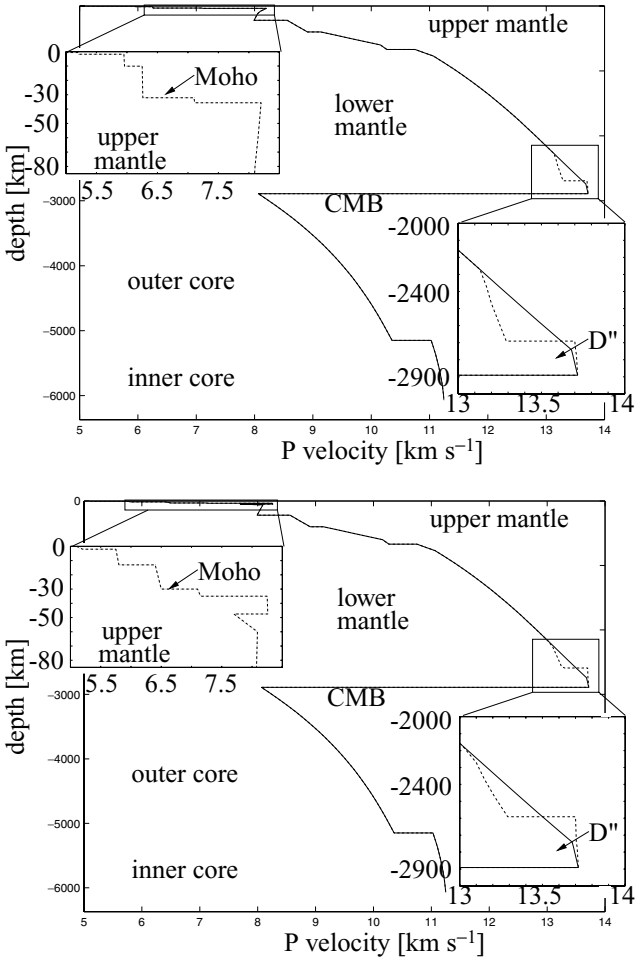

Figure 6. (a) Model used to compute synthetic data for comparison with data recorded at station DAWY. The reference model is PREM, the crustal structure (dash-dotted line) was taken from Lowe & Cassidy (1995). The discontinuity at the top of D″ was chosen to be 210 km above the CMB with a velocity contrast of 3 per cent compared to PREM in the model with D″ discontinuity (dashed curve). (b) Same as (a) but for station INK. The crustal model (dash-dotted line) was taken from Cassidy (1995). The top of the D″ discontinuity was chosen to be 310 km above the CMB which is similar to the model PWDK (dashed line).

resolution is much decreased compared to Figs 5(b) and (c) (error: ±1 s/°), also *PcP* and the Moho multiple merge as can also be seen in the real data and picking of the slowness becomes much more difficult.

The source vespagram for the station INK is shown in Fig. 7. The Moho multiple is predicted from the model of the crustal structure beneath INK determined by Cassidy (1995) (Fig. 6b). The *P* slowness for this distance range is 5.8 s/° and has been assigned to the data. Again all measurements have been made relative to the *P* wave values. The theoretical arrival time for *PcP* is 14 s after *P* and has a slowness of 4.3 s/° (4.3 (±1.5) s/° in the data, 13.5 s after *P*). The data show an arrival 6.75 s after *P* with a slowness of 5.5 (±1.2) s/°. If this arrival is interpreted as *PdP* the traveltime corresponds to a D″ thickness of 310 km (±15) which is slightly higher than the model PWDK. Again the velocity increase at D″ is modelled as 3 per cent and is comparable to the model PWDK (Weber & Davis 1990) (Fig. 7c) and for

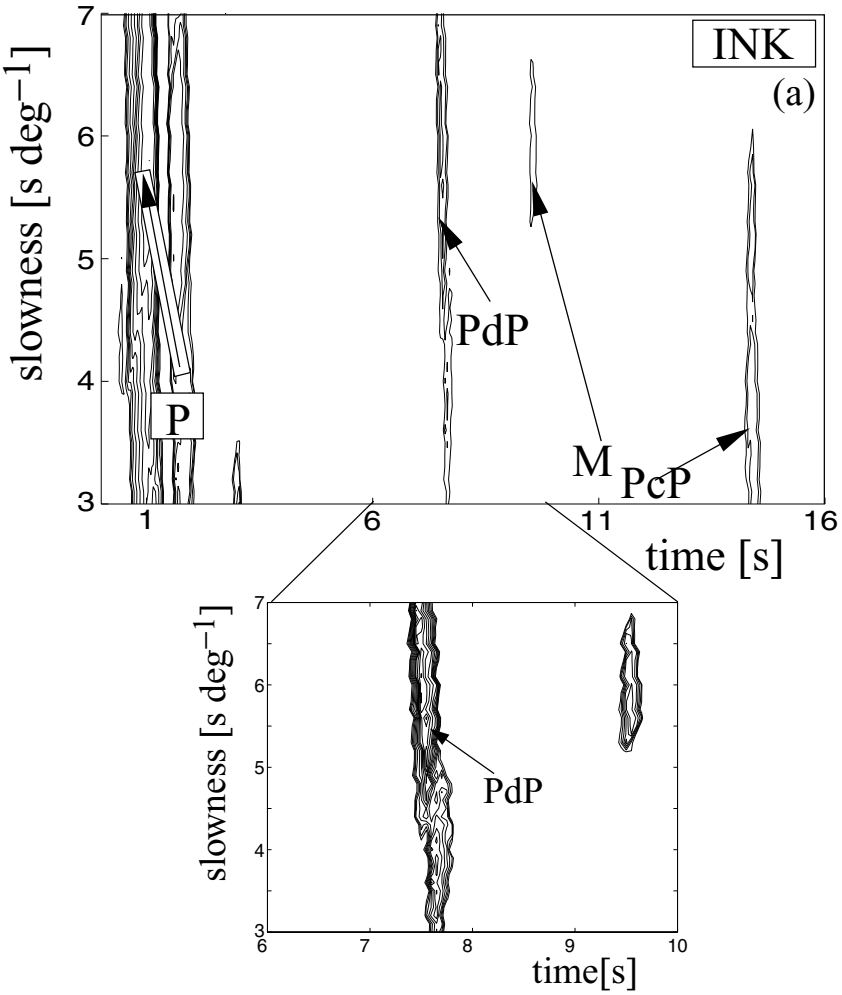

Figure 7. (a) A vespagram with real data (as in Fig. 5a) but for the CNSN station INK (average epicentral distance of 74°). Events 2–10, 13–15 and 18–19 are used for this vespagram. A phase which is interpreted as *PdP* can be seen roughly 7 s after *P*. The *P* to *S* conversion at the Moho (PmS) and the Moho multiples also appear in this vespagram. Contours as in Fig. 4. (b) Vespagram of synthetic data (as Fig. 5b) but for station INK using the model shown in Fig. 6(b) without a D″ discontinuity. (c) as (b) but for the model with D″ discontinuity. The reflection from the top of this discontinuity arrives 7 s after *P* for a reflector 310 km above the CMB. (d) As (c) but for a smaller array (40 km, 7 'sources').

comparison a vespagram with synthetic data for the model without a reflector at the top of D″ are shown (Fig. 7b). The prediction of the arrival time of *PdP* agrees well with the observations in Fig. 7(a).

The source vespagram of FRB (Fig. 8) shows *PdP* again 7.35 s after *P* with a reduced slowness compared to *P* of 5.2 ± 0.4 s/° (*P* is set to a slowness of 5.7 s/°). The slowness resolution in this vespagram is better compared to that for the INK vespagram since the great circle azimuth for this source–receiver combination strikes the long axis of the source-array at a more oblique angle. The *PdP* phase has a similar arrival time to that observed at the station INK, and traveltime modelling suggests a discontinuity again 290 ± 15 km above the CMB. At this time we do not have a crustal model for FRB so we cannot calculate synthetic vespagrams for this station.

It is worth noting that the slowness resolution in the three source vespagrams is not as good as that in the receiver vespagram generated using the German data (Fig. 4) due to the unfortunate orientation of the source array with respect to the great circle path to the Canadian stations as explained above.

4 F–K ANALYSIS

The vespagrams show signals which are consistent with reflections from a D″ discontinuity but in some cases the resolution is not sufficient to give an accurate estimate of slowness. This is somewhat due to the geometry of the source array as described above. There is also the question of how much these phases deviate from the source–receiver plane. Such deviations in azimuth would also distort the vespagram estimates of slowness. An alternate approach involves the analysis of the slowness and azimuth of the *PdP* phases in the frequency (*f*)—wavenumber (*k*) domain. The data are transformed to the $f - k$ domain using a 3-D Fourier transform; one transform to frequency and a double transform to the wavenumber domain k_x and k_y. In this domain the slowness and azimuth of a phase can be determined simultaneously (e.g. Capon 1973). Such analysis to our knowledge has only been used a few times to study D″ structure, (e.g. Weber 1993), but has been used to a limited extent to study other teleseismic phases (e.g. Murphy *et al.* 1997; Rost & Weber 2001) and local events (e.g. Spudich & Bostwick 1987).

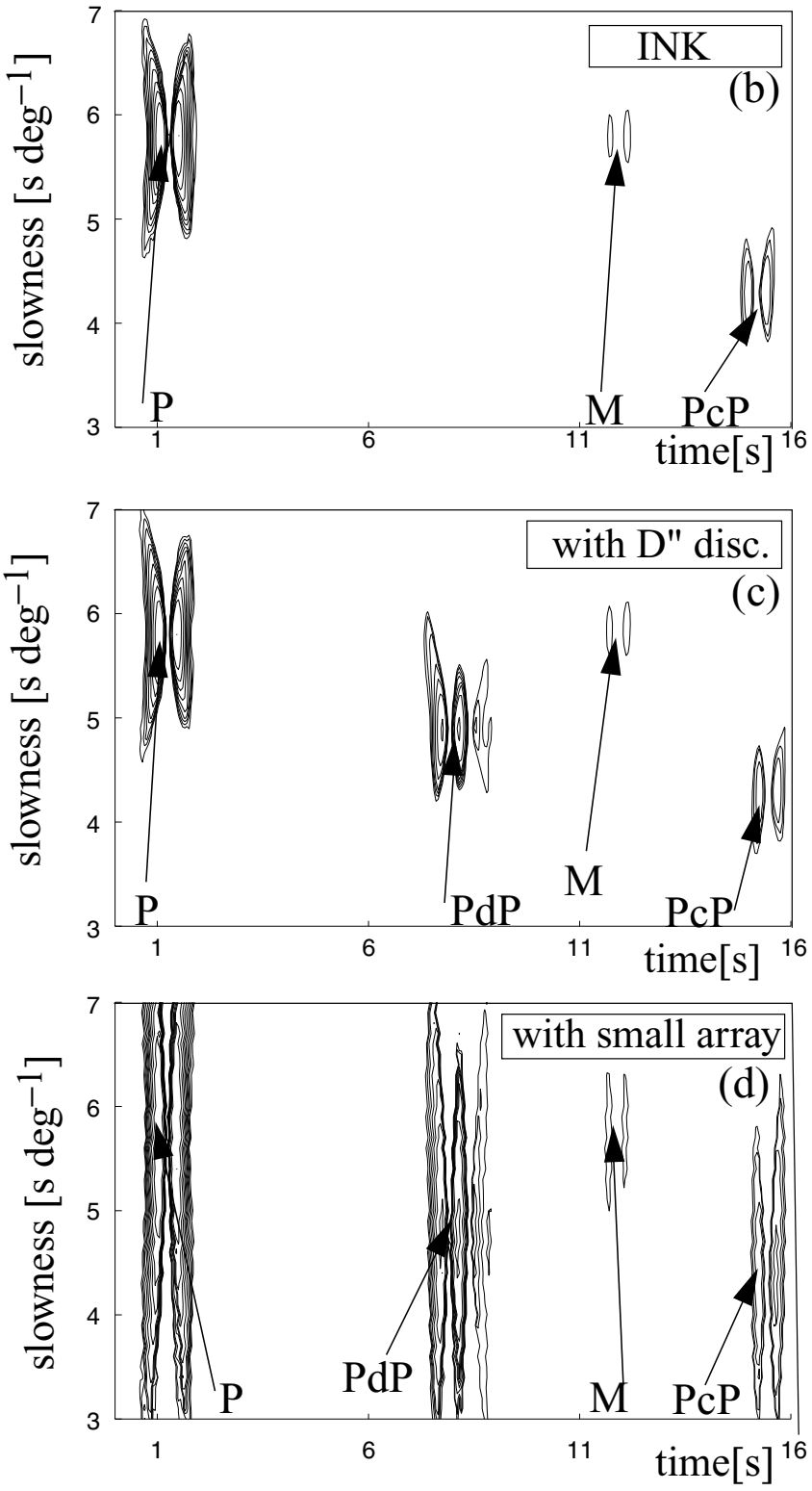

Figure 7. (*Continued*).

Fig. 9(a) shows the array response function (ARF) of the source array for 1 Hz waves. The ARF shows that, if waves arrive from North or South, the slowness resolution will be poor but the azimuth resolution will be good. In comparison, the ARF of the GRF-array is shown in Fig. 9(b). Here, the resolution of the slowness is better for the events arriving from an azimuth of ca. 30° (Kuriles to Germany) compared to Fig. 9(a).

We have applied $f - k$ analysis to the *P* and *PdP* phases observed at stations DAWY, INK and FRB. The results are shown in Fig. 10 for DAWY, Fig. 11 for INK and Fig. 12 for FRB. At

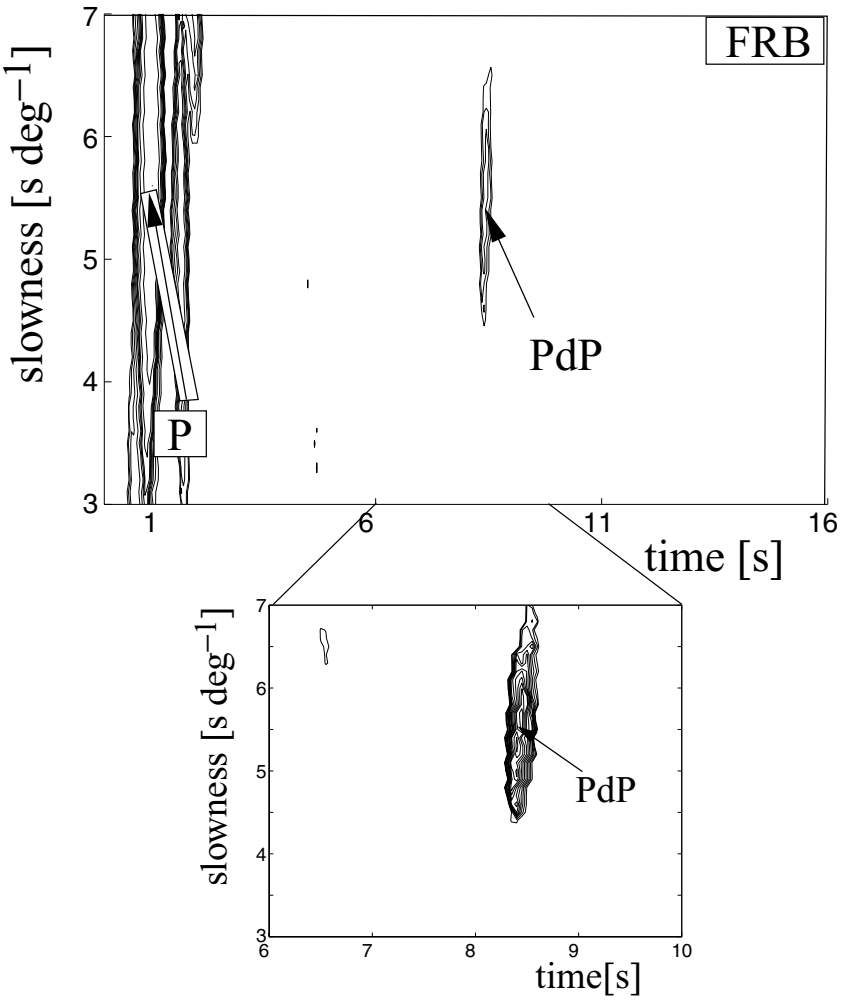

Figure 8. As Fig. 5(a) (real data) but for station FRB. For this vespagram events 1–4, 7–10, 14–16 and 18 were used. *PdP* arrives 7.35 s after the *P* arrival. Contours as in Fig. 4.

DAWY, *P* arrives with a slowness of 5.6(±0.8) s/° and backazimuth of 12.7(±5)°. These values correspond to the theoretically predicted values and demonstrate the applicability of $f-k$ analysis with such an array configuration (many events recorded at one station). The error of slowness and backazimuth in an $f-k$ analysis is the length and width, respectively, of the first contour line. The errors in the $f-k$ diagram are dependent on the ARF (Fig. 9a) which is elongated in N–S direction for the source array. The result for the *PdP* phase gives a slowness value of 5.2 (±1.2) s/° and a backazimuth of 12.2 (±8)°. This slowness reduction of *PdP* compared to *P* lends support to our interpretation of this phase as reflection from D″. The backazimuth difference between *P* and *PdP* is small, an indication that *PdP* travels very close to the great circle path for this source–receiver combination.

In the $f-k$ diagram for station INK (Fig. 11), a slowness value (u) of 5.8(±0.8) s/° and a backazimuth (baz) of 9(±5)° is measured for the *P* wave. For *PdP*, u is 5.2(±2.5) s/° and the backazimuth is 8(±13)°. The slowness resolution for *PdP* is less compared to the result for DAWY which is probably due to less coherency. Note that the slowness resolution is also poor in the vespagram for INK.

The $f-k$ analysis for station FRB (Fig. 12) shows *P* with a slowness of 5.7(±1) s/° and a backazimuth of 342(±5)°. The *PdP* phase shows a less coherent result than that for DAWY, but the analysis estimates a *PdP* slowness of 3.9(±2.5) s/° and a backazimuth of 327(±35)°. It is important to consider the shape of the ARF when interpreting results from $f-k$ analyses in that the contour-lines in an $f-k$ plot must exhibit a similar shape to the ARF. The $f-k$ plot in Fig. 12(b) shows a similar shape to the ARF adding confidence that our estimates are correct within the error bars. *PdP* deviates 15° from the great circle path implying that the D″ region may have considerable lateral variations in structure in this area. Such structure will affect the slowness estimate and although the travel-times from the vespagram suggest a 290 km thick D″ layer, the low slowness values (3.9 s/° versus 4.9 s/° for the model PWDK) suggest significant dip on this boundary or a reflection point different from the theoretical bounce point. This would also have an influence on the traveltime. We will come back to this point in the discussion. Another possibility is that the phase distortion of *PdP* and *PDP* (the diving wave) can have an effect of the slowness estimate (Murphy *et al.* 1997) although the aperture of our source array is small enough to avoid this.

We have also applied $f-k$ analysis to the GRF data (Fig. 13). Here the *P* phase shows a slowness of 5.6(±0.5) s/° and a backazimuth of 26.8(±11)°. The slowness of the *PdP* phase is 4.9(±0.5) s/°

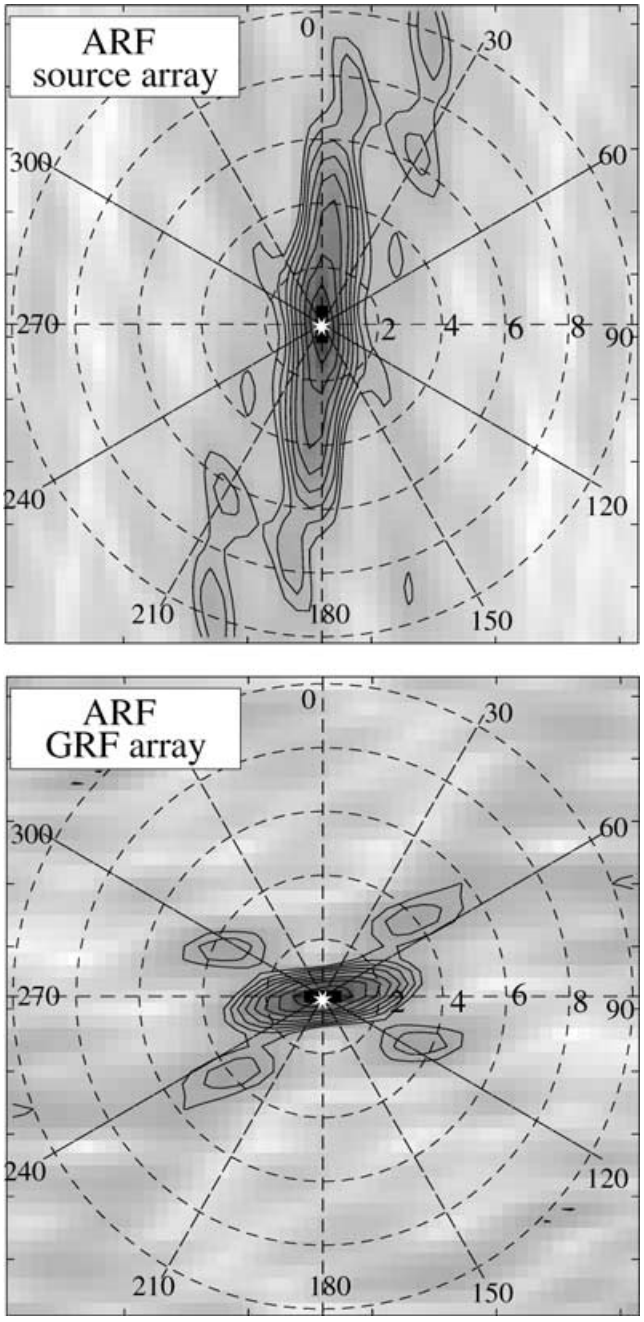

Figure 9. Array response function (ARF) for the source array (a) and for the GRF array (b) for a 1 Hz signal. Contour lines give energy in −1dB lines. The aperture and orientation of the arrays characterise the ARF. In the case of the source array, the slowness resolution will be less for waves in N–S direction (Canada to Hindu Kush) whereas for the GRF array the slowness resolution is good for events from the Kurile Island region (backazimuth around 25°).

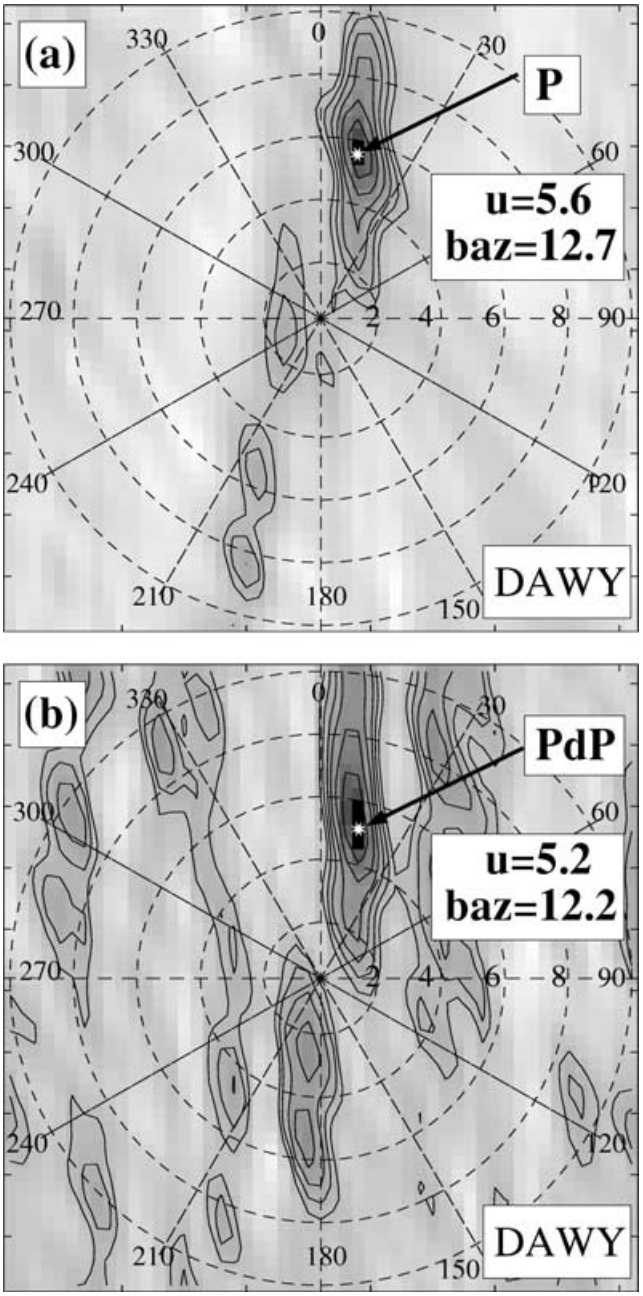

Figure 10. (a) Source $f-k$ analysis of the *P* wave (14 events recorded at station DAWY). The slowness (u) of 5.6 s/° and backazimuth (baz) of 13° was assigned to the *P* wave. The values found with the $f-k$ analysis are 5.6 (±0.8) s/° for the slowness and 12.7 (±5)° for the backazimuth. Contour lines give energy in −1dB spacing relative to the maximum amplitude (indicated by the white star). For the error, the first contour line was chosen in all $f-k$ diagrams. (b) as (a) but for the *PdP* phase. The slowness value is 5.2(±1.2) s/° and the backazimuth value is 12.2(±8)°. The slowness reduction of *PdP* versus *P* indicates that the phase originates from a reflection in the lowermost mantle.

with a backazimuth of 27.8(±11)°. The errors for the GRF results are smaller due to the ARF of this array compared to the ARF of the source array. For the Kurile–Germany path there is essentially no deviation from the great-circle path in either phase. The $f-k$ analysis shows that *PdP* arrives with the traveltime, slowness and the azimuthal emergence angle expected for a 1-D structure. Therefore, it seem reasonable to assume a 1-D structure.

5 DISCUSSION AND CONCLUSIONS

Observations of *PcP* precursors which sample a region beneath northern Siberia from almost orthogonal source–receiver paths provide a unique way of verifying the existence of a D″ discontinuity. The surface projections of reflection points from the top of this

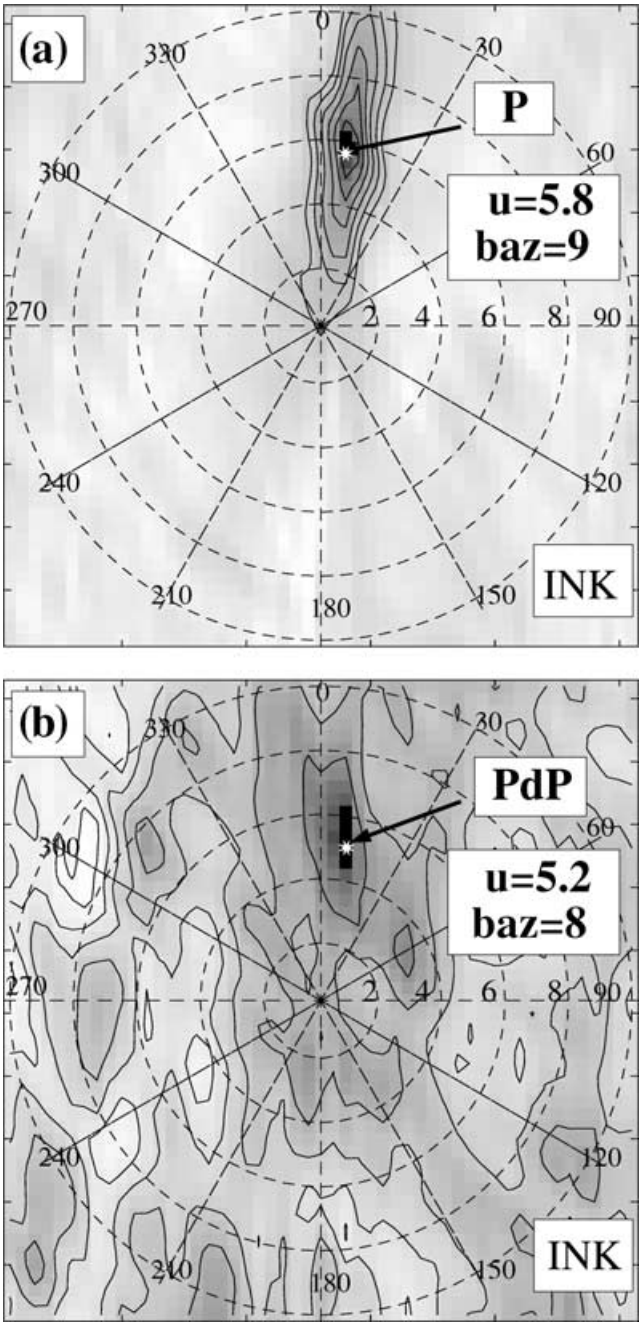

Figure 11. (a) Source $f-k$ analysis of the *P* wave as shown in Fig. 10 for 14 events recorded at station INK. The slowness of 5.8 s/° and backazimuth of 9° was assigned to the *P* wave. The error is ±0.8 s/° for the slowness and ±5° for the backazimuth. Contour lines as in Fig. 10. (b) as (a) but for the phase *PdP*. The slowness value is 5.2(±2.5) s/° and the backazimuth value is 8(±13)°. The resolution for this phase is poor, which may be due to a less incoherent *PdP* wave. Note that for the vespagram for INK the slowness resolution was poor as well.

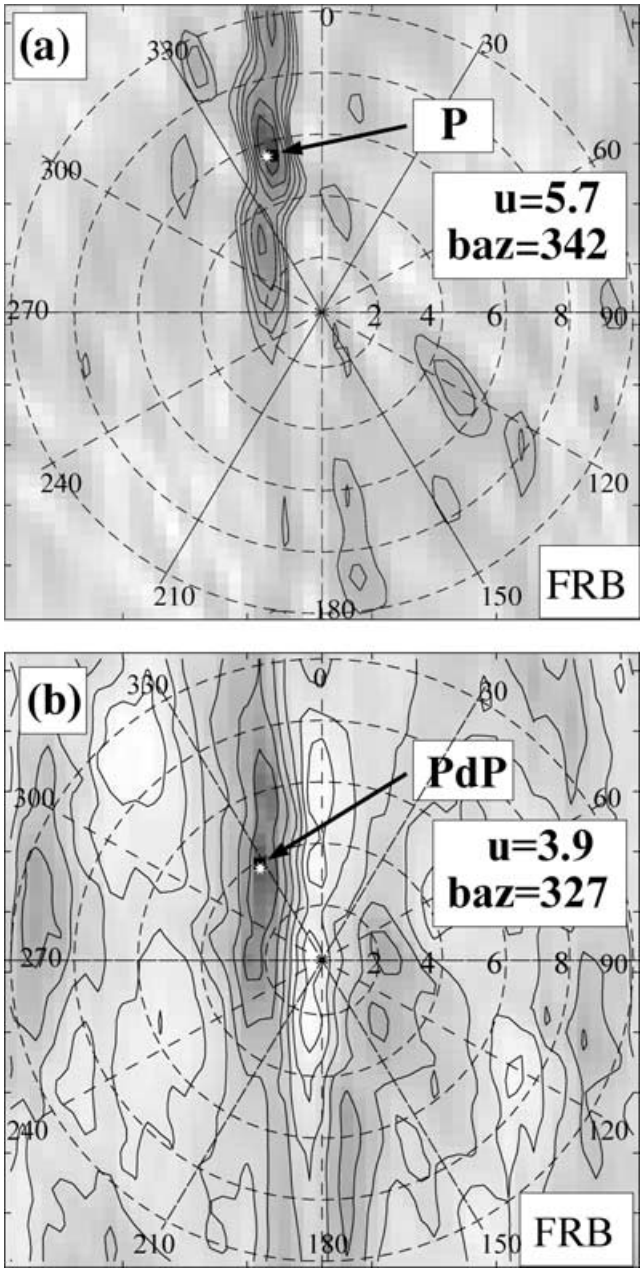

Figure 12. (a) Source $f-k$ analysis of the *P* wave as shown in Fig. 10 (12 events recorded at station FRB). The slowness of 5.7 s/° and backazimuth of 342° was assigned to the *P* wave. (b) as (a) but for the phase *PdP*. The slowness value is 3.9(±2.5) s/° and the backazimuth value is 327(±35)°. The difference in backazimuth indicates that *PdP* does not travel along the great circle path.

discontinuity for each of our studied source–receiver combinations are shown in Fig. 14. The grey triangles show the geometric bounce points from the Hindu-Kush events recorded at INK, the grey stars show bounce points for FRB and the grey circles show the bounce points for DAWY. Also shown (crosses) are the bounce points from Thomas & Weber (1997) for Japan and Kurile events recorded in Germany which include the bounce points for the Kurile events reanalysed here. The area sample by Hindu-Kush events recorded at the station INK overlaps with that studied by Thomas & Weber (1997) for the orthogonal path between northwest-Pacific events and Germany. The reflection points for stations DAWY and FRB sample previously untested regions. The size of the Fresnel zone for *S*-wave which sample this region is shown in Fig. 14. Our sample points do not overlap in terms of resolution. However, structure on length scales smaller than a Fresnel zone have been observed in

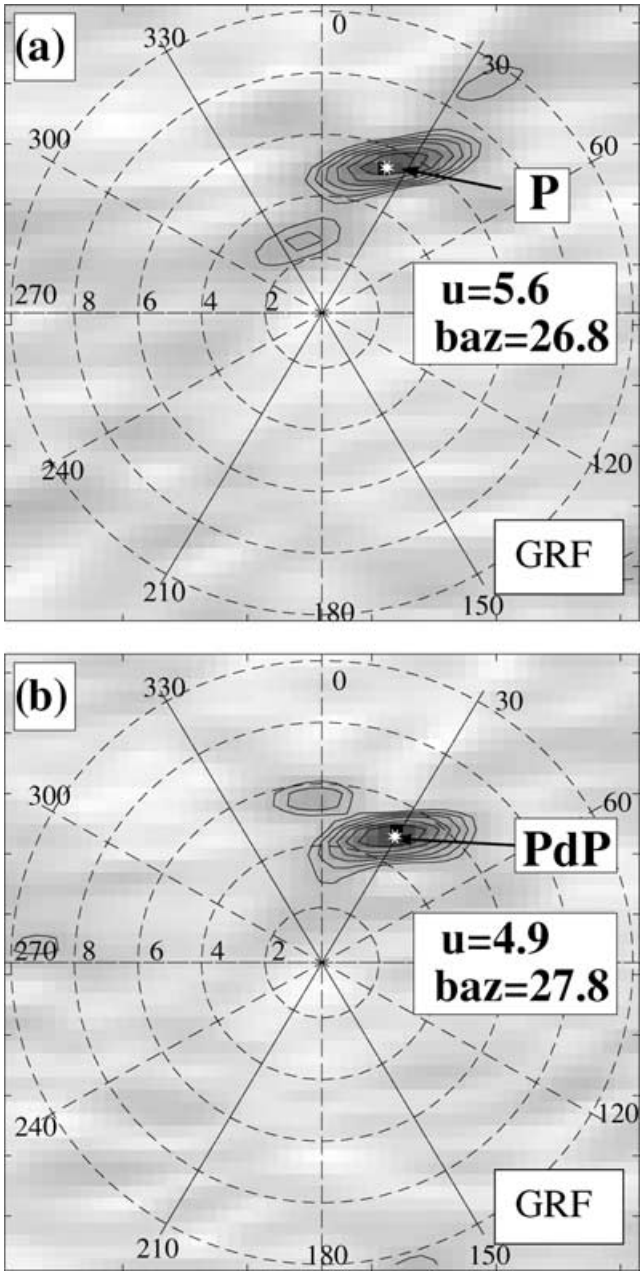

Figure 13. (a) Receiver $f-k$ analysis of the *P* wave as shown in Fig. 10 for GRF recordings of event 20. The slowness value is 5.6(±0.5)s/° and the backazimuth is 26.8(±11)°. (b) as (a) but for the phase *PdP*. Here the slowness is 4.9(±0.5) s/° and the backazimuth is 27.8(±11)°.

the D″ region (see Weber (1993) and Kendall & Shearer (1994) for discussion).

Values of slowness and backazimuth estimated from the vespagrams and $f-k$ analyses and the theoretical predictions are summarised in Table 2 for the phases *P*, *PdP* and *PcP* recorded at the GRSN and the 3 CNSN stations. There is a general agreement between the 3 estimates (theoretical value, estimates from the $f-k$ analysis and vespagram) at each array (source or receiver). There is though a wide range of values for *PdP* recorded of FRB, which may be due to a significant deviation (15°) from the source–receiver plane as suggested by the $f-k$ analysis. The accuracy of slowness estimates from the vespagrams and $f-k$ analyses depends on the geometry and aperture of the array and the dominant wavelength of the signal.

Source vespagrams of Hindu-Kush events recorded at the Canadian station INK yield estimates of a 310(±15km) km thick D″ layer which is similar to that obtained from receiver vespagrams of Japan and Kurile events recorded at German stations 293(±10) km. Our results from the Canadian station DAWY indicate that the layer thins to ∼210(±15) km in a region 3° (approximately 180 km at the CMB) to the east (a distance roughly the size of a Fresnel zone). This is in agreement with the results of Scherbaum *et al.* (1997) who found a similar trend of thinning to the East in a area north of the region sampled by the station INK. Furthermore, although these results are for *P*-waves, they generally agree with the results of Kendall & Shearer (1994) who looked at *S*-wave reflections in this area. They found a similar variation (200 to 300 km) in reflector distance from the CMB.

If the traveltime of *PdP* compared to *P* for the station FRB is used to estimate a reflector thickness, the results agree with the model PWDK although the reflection points lie in a previously unmapped region 16° (approximately 970 km at the CMB) west of the region mapped by INK and DAWY. That would suggest that the D″ discontinuity extends well west of the region previously studied by, for example, Lay & Helmberger (1983), Weber (1993) and Thomas & Weber (1997). FRB on the other hand is the only station which shows a large azimuthal deviation from the great-circle path. Our results from $f-k$ analysis yield slowness and azimuth estimates which can be used to more accurately locate the reflection point. 3-D ray tracing based on these values suggests a more southerly location of the reflection. Fig. 15 shows the reflection points for the measured slowness and backazimuth for 4 reflector depths (2800 km, 2700 km, 2600 km, 2500 km). Only a reflection from a depth of 2800 km gives the correct delay time with respect to the time arrival (7.36 s predicted, whereas the traveltime difference between *P* and *PdP* for FRB is 7.35 s). In this way we can use the travel-time, slowness and azimuth results to obtain a self-consistent result which is added into Fig. 14.

The large-scale topography found here has been interpreted as the result of the interaction of cold subducted material (the now extinct Izanagi or Kula plate Lithgow-Bertelloni & Richards 1998) with D″ beneath Siberia (Scherbaum *et al.* 1997). Possible scenarios which could explain the observed large variations in D″ topography are laminated or buckled subducted oceanic crust (Christensen & Hofmann 1994) and/or the resulting lateral displacement of D″ material.

An interesting observation is that the reflection points for the measured slowness and backazimuth values and traveltime for station FRB are close to a region where Thomas *et al.* (1999) found evidence of lower mantle scatterers from studies of precursors to *PKPdf* recorded at the German GRF-array and the GRSN. Other studies of scattered *PKPdf* precursors (e.g. Vidale & Hedlin 1998; Wen & Helmberger 1998) sample a region further north-east from the region shown here. Note that in the latter two studies there is some ambiguity as to whether the scatterers lie on the receiver side in the mantle beneath Europe or on the source side in the mantle beneath the *SW* Pacific. The region which was studied by Thomas *et al.* (1999) is shown in Fig. 14 as grey contoured area where the black region shows the most likely location of scatterers found within this area. One of the scatterers is about 10° (600 km at the CMB) to the west of the non geometrical reflection points for station FRB.

One possible explanation for the observations is that *PdP* is a reflection from discrete scatterers located within the lower mantle.

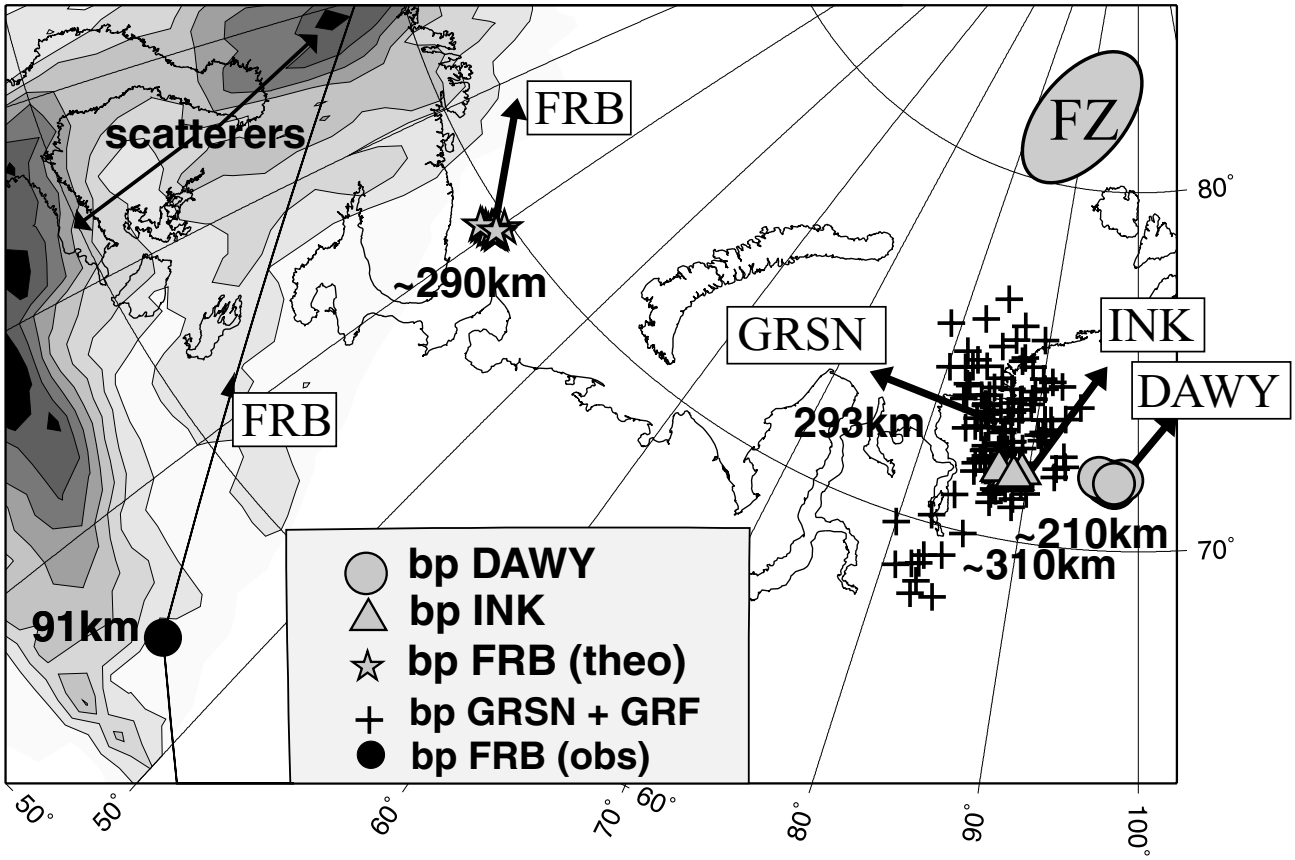

Figure 14. Surface projections of the reflection points at the top of D″ with the corresponding distances of the reflector from the CMB. The crosses are reflection points for the Kurile and Japan events recorded in Germany (Thomas & Weber 1997). The grey symbols are geometric reflection points for the Hindu-Kush to Canada paths (triangles: INK, circles: DAWY, stars: FRB). The arrows extending from the symbols show the direction of the great circle path to the receivers. The black circle in the bottom left corner shows the reflection point for station FRB using slowness, backazimuth and traveltime values from this study. The grey ellipse shows the 1D Fresnel zone (FZ) for 1 Hz data aligned with the Hindu-Kush to DAWY (INK) paths. The grey shaded area west of the geometric reflection points for station FRB shows the area where Thomas *et al.* (1999) have searched for scatterers and the black areas within this region show the location of isolated scatterers found with a migration method. This result is for a layer 1 km above the CMB.

This seems unlikely in most cases because of the coherency of the *PdP* observations in some large areas using, for example, the GRSN data (see the crosses in Fig. 14). Also, scatterers are often explained by inclusions of partial melt (e.g. Vidale & Hedlin 1998) and would therefore have a negative velocity contrast. In general the velocity contrast at the D″ reflector must be positive to explain the variations in *PdP* waveforms in the distance range 70° to 100° (e.g. see Weber & Davis 1990, or Kendall & Nangini (1996)). Nevertheless there have been suggestions that, in places, the D″ reflections may result from thin low-velocity lamellae within D″ (Weber 1994; Thomas *et al.* 1998). However, with the data set used in this study (Hindu-Kush events) we are unable to make a statement about the waveforms of *PdP* since the *PdP* signal in the raw traces is hidden in noise. Another interpretation is that the *PKP* scattering is due to small-scale topography on the D″ discontinuity. Variations in *PdP* on a small scale can be explained with small-scale topography (e.g. Thomas & Weber 1997). This interpretation would assume that the velocity contrast of the scatterers is positive. The third possibility is that the D″ region is very inhomogeneous, containing a discontinuity as well as small-scale scatterers which may or may not be inclusions of partial melt.

In the region where the scatterers are located, Garnero *et al.* (1998) have found evidence for ultra-low velocity zones. However in the region where a D″ discontinuity is observed (Thomas & Weber 1997; Weber 1993; Lay & Helmberger 1983; Gaherty & Lay 1992), Garnero *et al.* (1998) found no evidence for an ultra-low velocity zone. These observations are consistent with the interpretation that the D″ region is laterally very inhomogeneous, sometimes bounded by a discontinuity and sometimes containing scatterers and ultra-low velocity zones. Whether these features are mutually exclusive on a global scale remains to be seen.

The amplitude of *PdP* relative to *P* is smaller for the source vespagrams and seismograms from the Hindu Kush events than it is for the Kurile receiver vespagrams. Thomas & Weber (1997) also noticed variations in *PdP* amplitudes over small length-scales in this region. We speculate that this is due to focusing and defocusing effects due to the variable small-scale D″ topography. Another scenario could be that anisotropy in the D″ region affects the amplitude of *P* reflections from the top of this region in different ways for different directions. In a companion paper we investigate the anisotropy in this region (Thomas & Kendall 2002).

Repeating this analysis for *S*-waves is difficult as the Hindu-Kush sources are very close together making it difficult to generate useful vespagrams for the lower-frequency *S*-waves There is poorer slowness resolution due to the larger *S*-wavelengths. A larger range of distances (a few degrees) is usually needed for meaningful *S*-wave vespagrams. It may be possible to use the more widely distributed shallow events in this region. Analysis of *S*-wave anisotropy, if any,

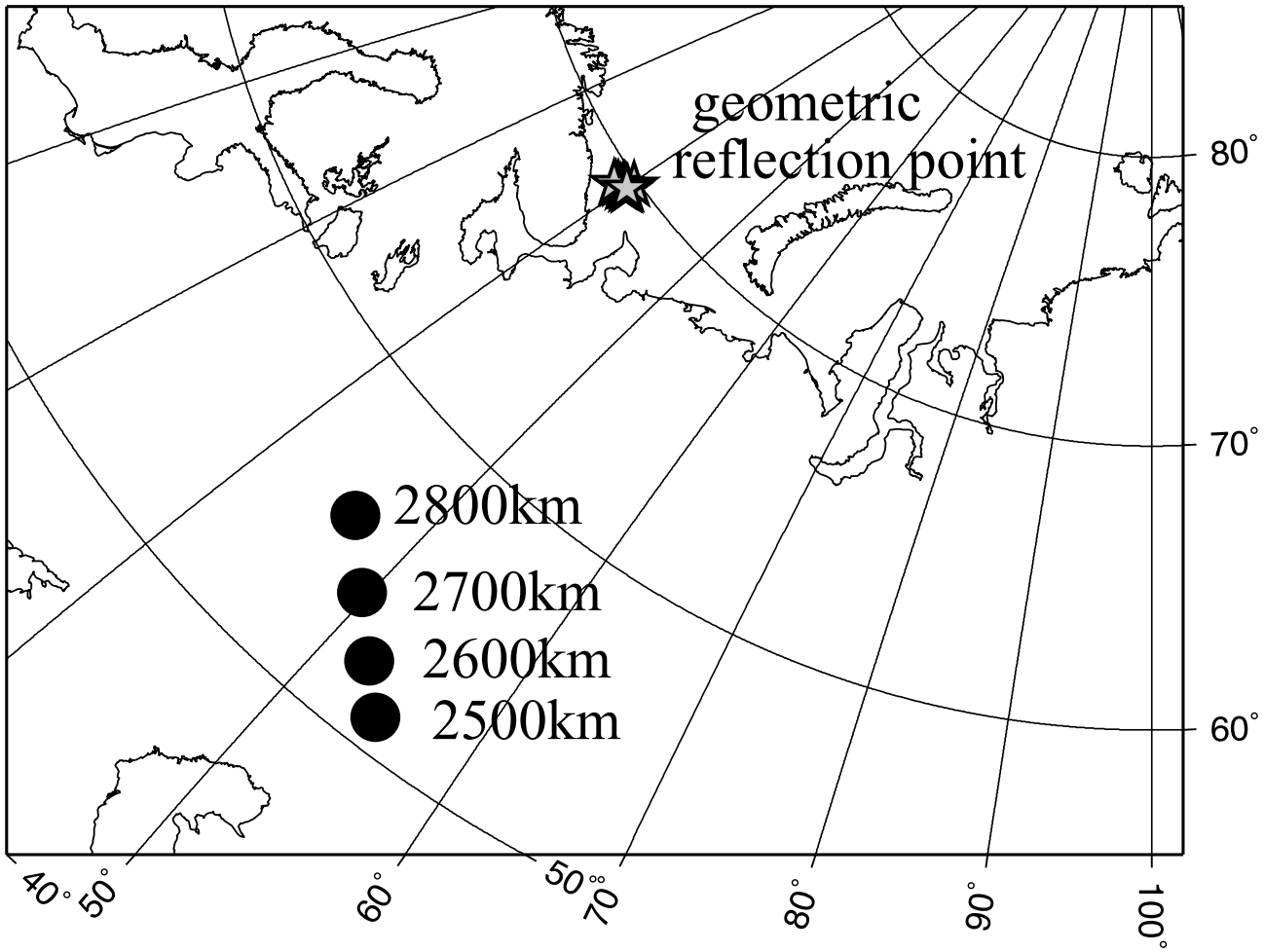

Figure 15. The reflection points of the *PdP* phase of station FRB calculated using slowness, backazimuth and traveltime information. The geometrical reflection points are shown as stars, the calculated reflection points are shown as circles. The depths for the reflection varies from 2800 to 2500 km. Only the reflection in 2800 km is able to explain the phase seen in the vespagram and $f - k$ analysis for station FRB.

is especially attractive as comparisons of *S*-wave splitting from orthogonal azimuths will provide strong constraints on the style of anisotropy in the region and is the topic of ongoing research.

ACKNOWLEDGMENTS

We would like to thank Bill Shannon and Wayne McNeil from the GSC and the staff from the SZGRF for providing the data from the CNSN, the GRSN and the GRF respectively. We also would like to thank K. Stammler and F. Krüger for programs to analyse and process the data and J. Cassidy for information on crustal structure beneath the CNSN stations. Part of this study was sponsored by the DAAD and the British Council. Maps have been produced using the programme GMT (Wessel & Smith 1991).

REFERENCES

Capon, J., 1973. Signal processing and frequency-wavenumber spectrum analysis for a large aperture seismic array, in *Methods in Computational Physics, 13,* pp. 1–59, ed. Bolt, B., Academic Press, New York and London.

Cassidy, J.F., 1995. A comparison of the receiver structure beneath stations of the Canadian National Seismograph Network, *Can. J. Earth. Sci.,* **32,** 938–951.

Christensen, U.R. & Hofmann, A.W., 1994. Segregation of subducted oceanic crust in the convecting mantle, *J. geophys. Res.,* **99,** 19 867–19 884.

Cleary J.R. & Haddon, R.A.W., 1972. Seismic wave scattering near the core mantle boundary: a new interpretation of precursors to PKP, *Nature,* **240,** 549–551.

Davies, D., Kelly, E.J. & Filson, J.R., 1971. Vespa process for analysis of seismic signals, *Nature Phys. Sciences,* **232,** 8–13.

Dziewonski, A. & Anderson, D.L., 1981. Preliminary reference earth model, *Phys. Earth planet. Int.,* **25,** 297–356.

Gaherty, J.B. & Lay, T., 1992. Investigation of laterally heterogeneous shear velocity structure in D″ beneath Eurasia, *J. geophys. Res.,* **97,** 417–435.

Garnero, E.J. & Helmberger, D.V., 1998. Further structural constraints and uncertainties of a thin laterally varying ultra low-velocity layer at the base of the mantle, *J. geophys. Res.,* **103,** 12 495–12 509.

Garnero, E.J., Revenaugh, J., Williams, Q., Lay, T. & Kellog, L.H., 1998. Ultra low velocity zones at the core-mantle boundary, in *The Core-Mantle Boundary Region, Geodynamic Series, 28,* pp. 97–118, eds Gurnis, M., Wysession, M., Knittle, E. & Buffett, B.A., American Geophysical Union, Washington DC.

Haddon, R.A.W. & Buchbinder, G.G.R., 1986. Wave propagation effects and the Earth's structure in the lower mantle, *Geophys. Res. Lett.,* **13,** 1489–1492.

Houard, S. & Nataf, H.-C., 1993. Laterally varying reflector at the top of beneath Northern Siberia, *Geophys. J. Int.,* **115,** 183–210.

Kendall, J.-M. & Shearer, P.M., 1994. Lateral variations in D″ thickness from long period shear wave data, *J. geophys. Res.,* **99,** 11 575–11 590.

Kendall, J-M. & Nangini, C., 1996. Lateral variations in below the Caribbean, *Geophys. Res. Lett.,* **23,** 399–402.

Krüger, F., Weber, M., Scherbaum, F. & Schlittenhardt, J., 1995. Normal and inhomogeneous lowermost mantle and core–mantle boundary under the Arctic and Northern Canada, *Geophys. J. Int.,* **122,** 637–658.

Lay, T. & Helmberger, D.V., 1983. A lower mantle S wave triplication and shear velocity structure of D″, *Geophys. J. R. astr. Soc.,* **75,** 799–838.

Lithgow-Bertelloni, C. & Richards, M.A., 1998. The dynamics of cenozoic and mesozoic plate motions, *Rev. Geophys.,* **36,** 27–78.

Loper, D.E. & Lay, T., 1995. The core mantle boundary region, *J. geophys. Res.,* **100,** 6397–6420.

Lowe, C. & Cassidy, J.F., 1995. Geophysical evidence for crustal thickness variations between the Denali and Tintina fault systems in west-central Yukon, *Tectonics,* **14,** 909–917.

Müller, G., 1985. The reflectivity method: A tutorial, *J. Geophys.,* **58,** 153–174.

Muirhead, K.J. & Datt, R., 1976. The *n*-th root process applied to seismic data, *Geophys. J. R. astr. Soc.,* **47,** 197–210.

Murphy, F.E., Neuberg, J.W. & Jacob, A.W.B., 1997. Alternatives to core mantle boundary topography, *Phys. Earth planet. Int.,* **103,** 349–364.

Rost, S. & Weber, M., 2001. A reflector at 200 km depth in the northwestern Pacific, *Geophys. J. Int.*, **147,** 12–28.

Scherbaum, F., Krüger, F. & Weber, M., 1997. Double beam imaging: mapping lower mantle heterogeneities using combinations of source and receiver arrays, *J. geophys. Res.,* **102,** 507–522.

Spudich, P. & Bostwick, T., 1987. Studies of the seismic coda using an earthquake cluster as a deeply buried seismograph array, *J. geophys. Res.,* **92,** 10 526–10 546.

Thomas, Ch. & Weber, M., 1997. P velocity heterogeneity in the lower mantle determined with the German Regional Seismic Network: Improvement of previous models and results of 2D modelling, *Phys. Earth planet. Int.,* **101,** 105–117.

Thomas, C. & Kendall, J-M., 2002. Images of D″ beneath northern Asia—II. Evidence for lower mantle anisotropy, *Geophys. J. Int.,* **151,** this issue.

Thomas, C., Weber, M., Hofstetter, R. & Agnon, A., 1998. A low velocity lamella in D″, *Geophys. Res. Lett.,* **25,** 2885–2888.

Thomas, Ch., Weber, M., Wicks, C. & Scherbaum, F., 1999. Small scatterers in the lower mantle observed at German broadband arrays, *J. geophys. Res.,* **104,** 15 073–15 088.

Vidale, J.E. & Hedlin, M.A.H., 1998. Evidence for partial melt at the core mantle boundary north of Tonga from the strong scattering of seismic waves, *Nature,* **391,** 682–685.

Weber, M., 1993. P and S-wave reflections from anomalies in the lower mantle, *Geophys. J. Int.,* **115,** 183–210.

Weber, M., 1994. Lamellae in D″? An alternative model for lower mantle anomalies, *Geophys. Res. Lett.,* **21,** 2531–2534

Weber, M. & Davis, J.P., 1990. Evidence of a laterally variable lower mantle structure from P- and S-waves, *Geophys. J. Int.,* **102,** 231–255.

Weber, M., Davis, J.P., Thomas, Ch., Krüger, F., Scherbaum, F., Schlittenhardt, J. & Körnig, M., 1996. The structure of the lowermost mantle as determined from using seismic arrays, in *Seismic Modeling of the Earth's Structure,* pp. 399–442, eds Boschi, E., Ekström, G. & Morelli A., Instituto Nazionale di Geophysica, Roma.

Wen, L. & Helmberger, D.V., 1998. Ultra low velocity zones near the core-mantle boundary from broadband PKP precursors, *Science,* **279,** 1701–1703.

Wessel, P. & Smith, W.H.F, 1991. Free software helps map and display data, *EOS Trans. Am. geophys. Un.,* **72,** 441, 445–446.